Design of a Lightweight Multilayered Composite for DC to 20 GHz Electromagnetic Shielding

Paul Clerico, Lionel Pichon, Xavier Mininger, Olivier Dubrunfaut, Chadi Gannouni, Delong He, Jinbo Bai, Laurent Prevond

electronics

MDPI

Article

Design of a Lightweight Multilayered Composite for DC to 20 GHz Electromagnetic Shielding

Paul Clérico [1,2,*], Lionel Pichon [1,2], Xavier Mininger [1,2], Olivier Dubrunfaut [1,2], Chadi Gannouni [1,2], Delong He [3], Jinbo Bai [3] and Laurent Prévond [4]

1 Laboratoire de Génie Electrique et Electronique de Paris (GeePs), CNRS, CentraleSupelec, Université Paris-Saclay, 91192 Gif-sur-Yvette, France; lionel.pichon@centralesupelec.fr (L.P.); xavier.mininger@centralesupelec.fr (X.M.); olivier.dubrunfaut@centralesupelec.fr (O.D.); chadi.gannouni@centralesupelec.fr (C.G.)
2 Laboratoire de Génie Electrique et Electronique de Paris (GeePs), CNRS, Sorbonne Université, 75252 Paris, France
3 Laboratoire de Mécanique des Sols, Structures et Matériaux (MSSMat), CNRS, CentraleSupelec, Université Paris-Saclay, 91190 Gif-sur-Yvette, France; delong.he@centralesupelec.fr (D.H.); jinbo.bai@centralesupelec.fr (J.B.)
4 SATIE–CNAM, CNRS, ENS Paris-Saclay, Université Paris-Saclay, 91190 Gif-sur-Yvette, France; laurent.prevond@lecnam.net
* Correspondence: paul.clerico@centralesupelec.fr

Citation: Clérico, P.; Pichon, L.; Mininger, X.; Dubrunfaut, O.; Gannouni, C.; He, D.; Bai, J.; Prévond, L. Design of a Lightweight Multilayered Composite for DC to 20 GHz Electromagnetic Shielding. *Electronics* **2021**, *10*, 3144. https://doi.org/10.3390/electronics10243144

Academic Editors: Slawomir Wiak, Paolo Di Barba and Lukasz Szymanski

Received: 8 November 2021
Accepted: 15 December 2021
Published: 17 December 2021

Abstract: The work aims to design a trilayer composite dedicated to electromagnetic shielding over a large frequency range, from 1 Hz to 20 GHz. Analytical and numerical models are used to determine the shielding effectiveness (SE) of this composite in the case of a planar shield. The shield is constituted of a support layer, a magnetic layer, and a conductive layer. Two possible designs are considered. To simplify the numerical calculation, a homogenization method and the Artificial Material Single Layer (AMSL) method are used. The proposed composite shows a good shielding capacity over the whole studied frequency range, with shielding effectiveness higher than 17 dB and 75 dB, respectively, in the near-field (1 Hz–1 MHz) and far-field (1 MHz–20 GHz). Both homogenization and AMSL methods show good suitability in near-field and allow one to greatly reduce the calculation time.

Keywords: electromagnetic shielding; shielding effectiveness; composite; low frequency; high frequency; near-field; far-field; finite element method

1. Introduction

In recent years, the growth of electrical and electronic industries led to the broadening of the frequency spectrum and the increase in different sources of electromagnetic disturbances. Both magnetic field and high-frequency electromagnetic radiation may then coexist in a practical working environment. Thus, it is necessary to provide adequate shielding solutions, which cover a wide frequency band.

Metals are widely used in shielding applications due to their high conductivity and/or permeability. Conductive metals are known to shield high-frequency electromagnetic fields [1,2] thanks to eddy currents. Magnetic metals are able to shield low-frequency electromagnetic fields [3–5] thanks to their capacity to channel magnetic flux. Multilayered shields or biphasic composite, combining both conductive and magnetic metals, give interesting results in different frequency ranges [6–10]. Indeed, the authors previously observed the magnetic shielding effectiveness of a 230 µm Al/steel/Al composite is 8 dB at 10 kHz, higher than a single 250 µm Al layer, which is 6 dB [6]. Similarly, Ma et al. [8] elaborated a 1 mm Fe/Al/Fe composite and showed its static magnetic shielding effectiveness is around 10 dB, about 2.5 times that of a pure iron plate. Moreover, its electromagnetic shielding effectiveness reaches 40–70 dB in the frequency range of 30 kHz–1.5 GHz. Watanabe et al. [9]

showed the shielding effectiveness of a stack of five Cu(0.7 μm)NiFe(0.3 μm) layers is 37.6 dB at 40 MHz, 3.9 times higher compared with a 5 μm copper layer.

However, metals generally have a high mass density, and in order to reduce the mass of equipment and pollution, recent studies are focused on lightweight composites in bulk or foam structures based mainly on metal foams [11], a polymer matrix with metallic particles [12,13], metallic fibers [14], metallic microwires [15–17], carbon nanotubes [18–20], carbon fibers [21,22], or graphene [23]. Carbon fillers are used in polymer composites for their lower conductivities than metallic fillers in order to reduce reflectivity. However, in counterpart, their shielding effectiveness is also lower. The electromagnetic shielding effectiveness of a 5 mm stainless-steel fibers/polymer composite is around 78 dB at 2 GHz with a filler content of 25 wt%, a fiber diameter of 8 μm, and an aspect ratio of 1000 [14]. A 2 mm ferromagnetic microwires-graphene/silicone elastomer composite has maximum shielding effectiveness of 18 dB at 8.2–12.4 GHz with a 0.059 wt% filler content [17]. In comparison, a 2 mm carbon nanotubes/epoxy foam composite has constant shielding effectiveness of around 23 dB between 12 and 18 GHz with a 5 wt% filler content [19]. Thus, to reach similar shielding effectiveness, the filler content must be higher for carbon fillers than with metallic fillers. Those composites are nevertheless less conductive than bulk metals and show lower shielding effectiveness. Moreover, most studies on those composites are only focused on a limited frequency range, and mainly at a high frequency (GHz). The use of those composites in near-field applications is therefore not assured.

Thus, a composite that joins lightness and capacity to shield a large frequency band is still to be studied. In this context, the novelty of this work is to design a wide-frequency-band, lightweight, multilayered, composite shielding structure that can perform at very low and high frequencies, from 1 Hz to 20 GHz. This paper studies the shielding effectiveness of a trilayer composite associated with a support layer (SL) used for mechanical strength, a metallic magnetic layer (ML) for low-frequency shielding, and a conductive layer (CL) for high-frequency shielding. Initially, two possible structures are considered: ML/SL/CL and SL/CL/ML. In both cases, the SL, ML, and CL thicknesses are 2 mm, 23 μm (+25 μm of adhesive), and 50 μm, respectively. Such thickness values correspond to many practical cases related to embedded enclosures in automotive or aircraft vehicles. The small thicknesses of the ML and CL ensure the lightness of the composite.

The shielding effectiveness of the composite is evaluated with analytical and numerical models. In order to study the shielding effectiveness for a wide frequency range, two analytical models are used: The Moser model [24] in the case of a near-field magnetic shielding at a low frequency and Schelkunoff decomposition [25] in the case of a far-field plane wave shielding at a high frequency. Both models give accurate results in their specific frequency range. For example, Kühn et al. [26] observed, in the case of an aluminum layer of 300 μm with an area of 0.3 m $\times$ 0.2 m, the near-field magnetic shielding effectiveness obtained from the Moser model is close to the experimental measurements, especially in the lower frequency range ($f < 1$ kHz). The frequency range $f < 2.5$ kHz is not described correctly by the Schelkunoff decomposition. Both the Moser model and Schelkunoff decomposition match the experimental results by 2.5 kHz to 200 kHz.

Moreover, two numerical models are also implemented in COMSOL Multiphysics: One with an AC/DC module for the near-field application and one with an RF module for the far-field application. Thin-layer modeling is quite challenging, especially for 3D applications. In order to simplify numerical calculations and consider integrating the proposed multilayered composite into future 3D models, a homogenization method [6] and Artificial Material Single Layer (AMSL) method [27] are used. The limits of these methods are determined by comparing the shielding effectiveness of the trilayer composite, the homogenized layer, and the artificial layer.

2. Materials and Electromagnetic Model

2.1. Materials

The SL, CL, and ML refer to a glass-fiber-reinforced epoxy composite, a graphene sheet, and a mu-ferro sheet, respectively. Mu-ferro is the commercial name for soft magnetic metal with a relative permeability within 10,000 and 25,000 at direct current [28]. The properties of these materials are resumed in Table 1. The conductivity is calculated from a resistivity measurement obtained by a four-probe method. The relative permeability of the mu-ferro sheet given in Table 1 corresponds to those calculated in the near-field at 1 Hz and 1 MHz from experimental measurements. Further details will be specified in Section 3.1. The change in permeability with frequency is considered in the developed model. For far-field applications (f > 1 MHz), its relative permeability is set to 1.

Table 1. Thickness, conductivity, and relative permeability of each layer.

Layer	Thickness	Conductivity (S/m)	Relative Permeability
SL (glass fiber/epoxy)	2 mm	1×10^{-12}	1
CL (graphene)	50 µm	6.8×10^{5}	1
ML (mu-ferro)	23 µm	4.8×10^{5}	14,200 (1 Hz) 1340 (1 MHz) 1 (>1 MHz)

2.2. Analytical Models

The analytical model of Moser [24] gives the shielding effectiveness (SE) for an infinite plane sheet illuminated by a magnetic field produced by a loop (near-field). In this model, the shield is centered between the emitting loop and the receiving loop. The SE is then defined as follows:

$$SE = 20\log_{10}\left|\frac{1}{4\mu_r}\frac{\int_0^{+\infty} x^2\tau_0^{-1}\mathcal{J}_1(xr)e^{-\tau_0 z}dx}{\int_0^{+\infty} Kx^2\tau\tau_0^{-2}\mathcal{J}_1(xr)e^{-\tau_0 z-(\tau-\tau_0)l}dx}\right| \quad (1)$$

$$K = \left[\left(\frac{\tau}{\tau_0}+\mu_r\right)^2 - \left(\frac{\tau}{\tau_0}-\mu_r\right)^2 e^{-2\tau l}\right]^{-1} \quad (2)$$

$$\tau = \sqrt{x^2-\gamma^2} \quad (3)$$

$$\tau_0 = \sqrt{x^2-\gamma_0^2} \quad (4)$$

$$\gamma = \sqrt{\varepsilon_0\varepsilon_r\mu_0\mu_r\omega^2 - j\mu_0\mu_r\sigma\omega} \quad (5)$$

$$\gamma_0 = j\frac{\omega}{c} \quad (6)$$

$\mathcal{J}_1$ is the Bessel function of the first kind of order 1, γ is the propagation constant in the shield, γ_0 is the free-space propagation constant, ω is the angular frequency, c is the free-space velocity of light, l is the shield thickness, r is the emitting loop radius, z is the distance between the emitting loop and the receiving loop, (ε_0, μ_0) are, respectively, the free-space permittivity and permeability equal to 8.854×10^{-12} F/m and $4\pi \times 10^{-7}$ H/m, and (ε_r, μ_r, σ) are, respectively, the relative permittivity, the relative permeability, and the conductivity of the shield. In all of our calculations, the relative permittivity is considered equal to 1.

The Schelkunoff decomposition [25] gives the SE for an infinite plane sheet illuminated by a normal incident plane wave (far-field). The SE is defined as follows:

$$SE = 20\log_{10}\left(e^{j\gamma l}\left|\frac{1}{1-\rho^2}\right|\left|1-\rho^2 e^{-2j\gamma l}\right|\right) \quad (7)$$

$$\rho = \frac{Z_m - Z_0}{Z_m + Z_0} \quad (8)$$

$$Z_m = \sqrt{\frac{j\mu_0\mu_r\omega}{\sigma}} \quad (9)$$

$$Z_0 = \sqrt{\frac{\mu_0}{\varepsilon_0}} \quad (10)$$

ρ is the reflection coefficient, Z_0 is the free-space wave impedance equal to 377 Ω, and Z_m is the shield impedance.

2.3. Numerical Models

The geometries of the two numerical models, corresponding to analytical models, are represented in Figure 1 for the near-field (a) and far-field (b) applications. For the near-field case, due to symmetry, the numerical model is developed in 2D-axisymmetric with the AC/DC module. A loop of a radius r of 1.5 cm illuminates the sample, modeled as a circular disc with a radius of 10.5 cm. The sample radius is 7 times the loop radius to approach the infinite plane assumption in the Moser model, which is not conceivable in this numerical model, while keeping an adequate computation time. The distance d between the loop and the sample and between the sample and the measuring point is fixed at 2 cm. A layer of infinite elements bounds the computational domain. The SE is calculated by computing the magnetic field on the symmetry axis with and without the sample.

For the far-field analysis, the numerical model is developed in 2D with the RF module. Two ports are defined, one emitting a transverse electromagnetic wave and one receiving it. Two layers of the Perfectly Matched Layer (PML) bound the model. The edges are defined as a Perfect Electric Conductor (PEC) for symmetry. The sample is in contact with the model edges to consider it as an infinite plane. The SE is directly related to the transmission loss S21dB.

Figure 2 shows a schematic diagram of the homogenization (a) and the AMSL (b) methods. The homogenization method, based on an energetic approach at a direct current [6], allows considering the trilayer composite as a homogenized layer with effective conductivity and permeability. Then, the AMSL method [27] allows considering the homogenized layer as an artificial layer where only one element mesh is required in the thickness for the numerical calculation, instead of a standard fine mesh discretizing the homogenized layer.

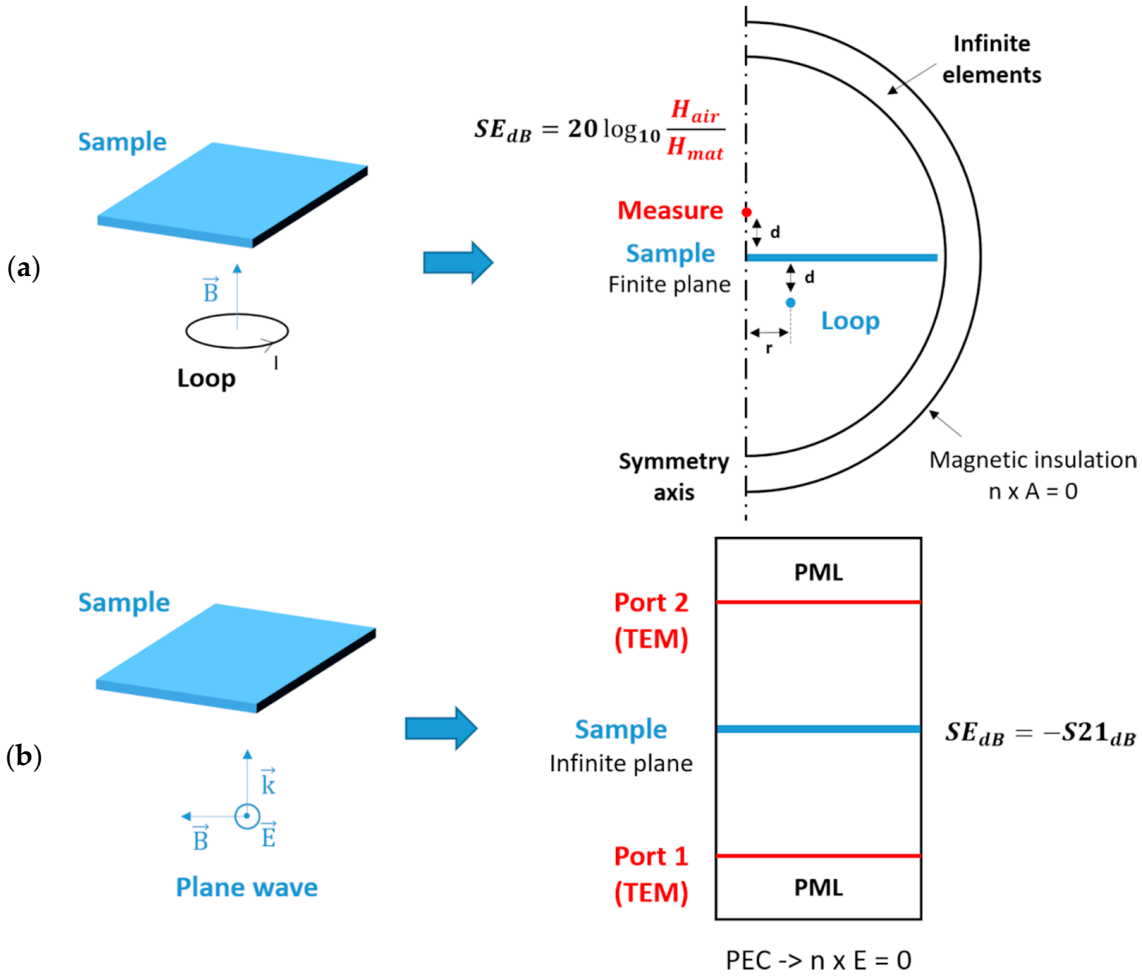

Figure 1. Schematic diagrams of the numerical model in the near-field (**a**) and far-field (**b**).

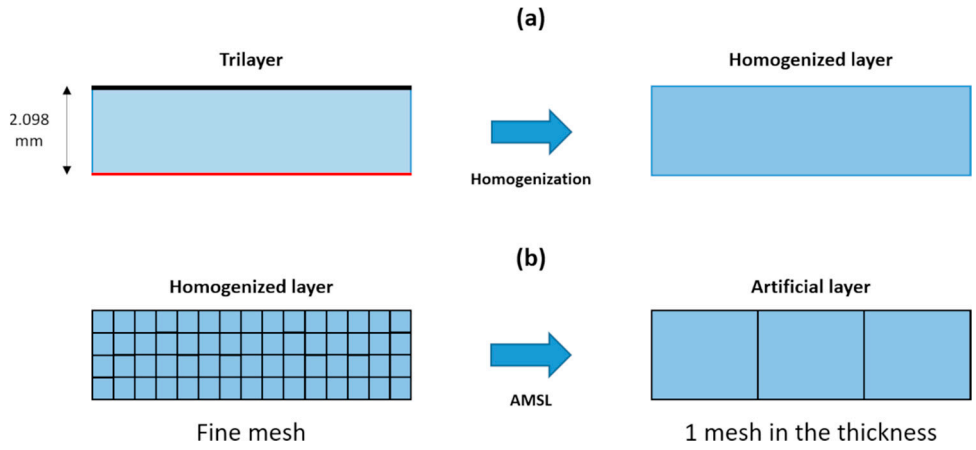

Figure 2. Schematic diagrams of the homogenization method (**a**) and the AMSL method (**b**).

3. Results and Discussion

3.1. Relative Permeability of the Mu-Ferro and SE of One-Material Sheet

The relative permeability of the mu-ferro sheet is determined from experimental measurements. The experimental SE is measured with a gain-phase analyzer (HP 4194A) from 10 Hz to 1 MHz. The permeability is calculated by minimizing the difference between the SE obtained numerically with the 2D-axi model and the experimental one. The resulting relative permeability, plotted in Figure 3a, is constant at 14,200, until around 2 kHz. For the

case of a distance d of 3.05 cm, the experimental SE and the SE obtained from the numerical model for both mu-ferro and graphene layers are plotted in Figure 3b. Experimental and numerical results show a good concordance from around 100 Hz where experimental measures are less noisy.

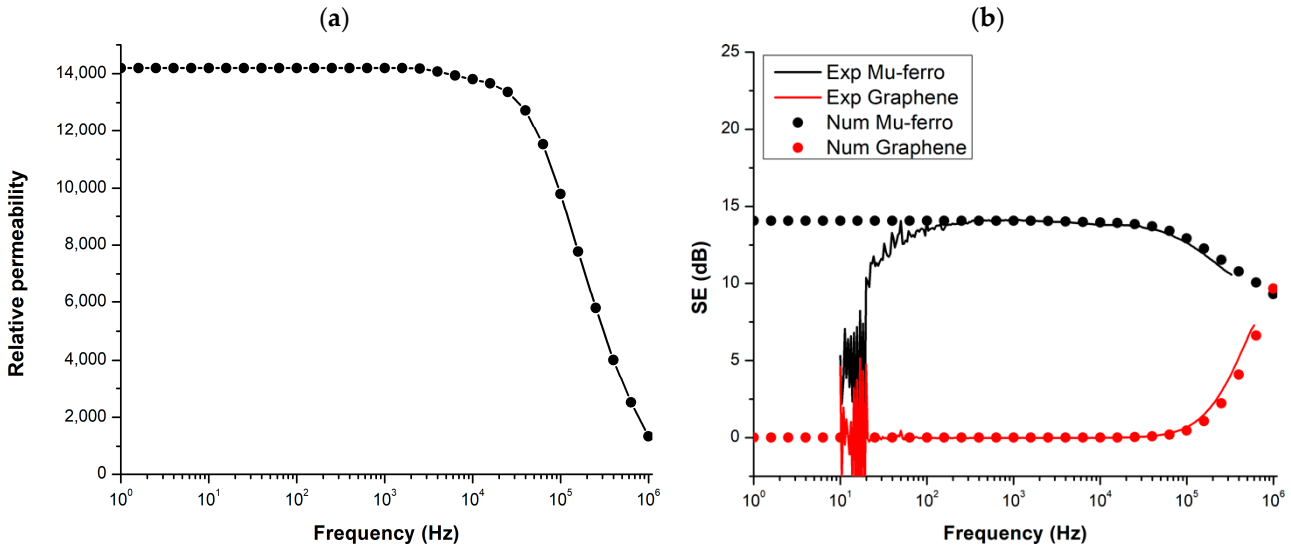

Figure 3. Measured relative permeability of the mu-ferro layer (**a**); experimental (line) and numerical (dot) shielding effectiveness of both mu-ferro and graphene layers for a distance d of 3.05 cm (**b**).

3.2. Layer Arrangements

Initially, two layer arrangements are considered: The first case where the CL and the ML are separated by the SL, and a second case where both layers are on the same side of the SL (Figure 4a). The SE for these two structures obtained numerically in far-field is plotted in Figure 4b. It is observed that the SE of the ML/SL/CL composite is greater than the SE of the SL/CL/ML composite for frequencies higher than 2 MHz. As expected, no difference between the two layers' arrangement is noted in the near-field for a low frequency.

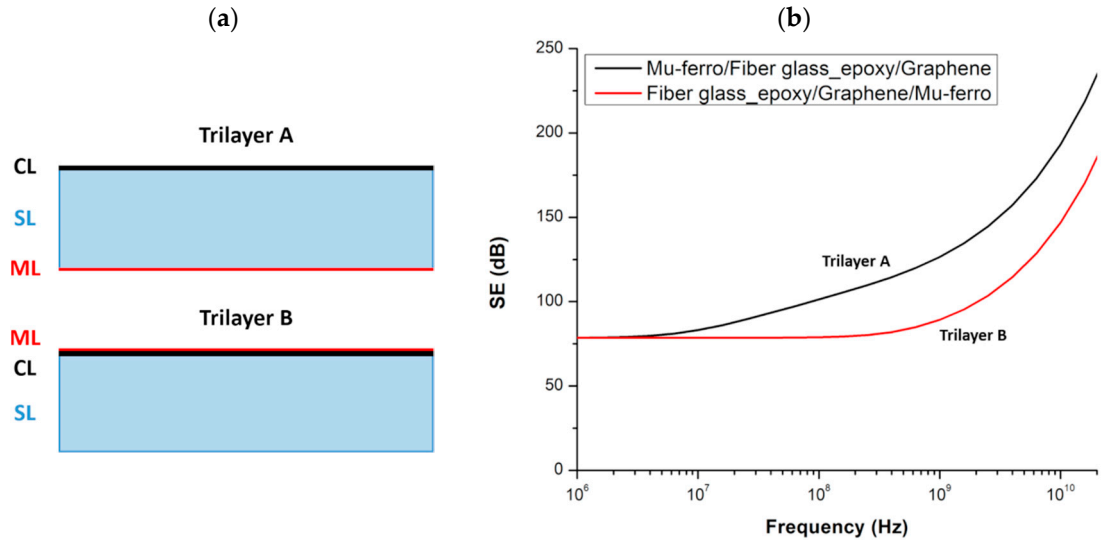

Figure 4. Schematic diagram (**a**) and shielding effectiveness (**b**) of both layer arrangements obtained in far-field with the numerical model.

3.3. Materials Contribution

The SE of the trilayer composite, a single graphene layer, and a single mu-ferro layer is calculated in near-field from 1 Hz to 1 MHz and in the far-field from 1 MHz to 20 GHz. The results of the numerical models are presented in Figure 5a,b, respectively, in the near-field and far-field.

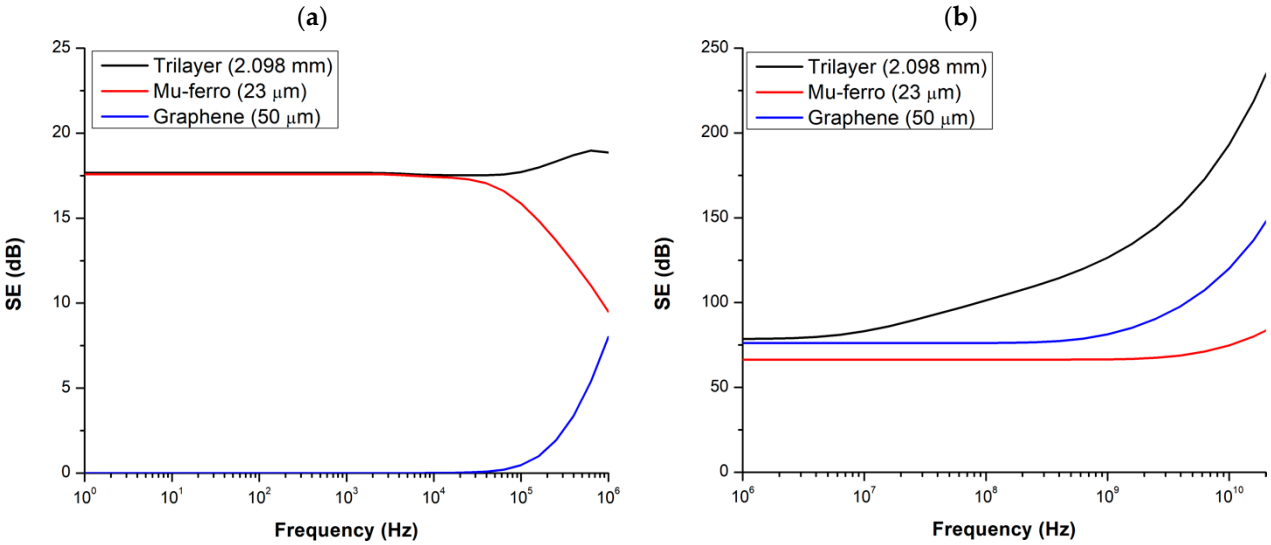

Figure 5. Shielding effectiveness of the trilayer composite (black), the graphene layer (blue), and the mu-ferro layer (red) obtained with the numerical model in the near-field (**a**) and far-field (**b**).

In the near-field, thanks to its high relative permeability, the mu-ferro layer has an SE of 17.6 dB from 1 Hz to 10 kHz that then decreases to 9.5 dB at 1 MHz. The SE of the graphene layer increases only from 20 kHz. The trilayer composite shows both interesting behaviors with the capacity to shield at a low frequency thanks to the mu-ferro layer. Above 20 kHz, the decrease in SE with the frequency is compensated by an increase thanks to the graphene layer.

In the far-field, as both graphene and mu-ferro layers are conductive, their SE is high enough. By combining both layers, the SE of the trilayer composite is greater than 75 dB for the whole frequency range.

Note that the SE at 1 MHz in the near-field is different from the one in the far-field due to the different assumptions of AC/DC and HF approaches. As a consequence, AC/DC and RF modules of COMSOL Multiphysics are limited to their respective range of frequencies and give accurate results only in those frequency bands.

3.4. Validity of Homogenization and AMSL Methods

The results of the analytical model and numerical model in the near-field are compared for the trilayer study in Figure 6. In the case of the numerical approach, the SE of the actual trilayer composite, the homogenized layer, and the artificial layer are plotted.

First, it should be noted that the Moser model was developed only for single layers and cannot be used for multilayers. Thus, in the near-field, the comparison between analytical and numerical models is performed with the homogenized layer. The SE of the homogenized layer obtained analytically with the Moser model and numerically presents a difference of around 0.9 dB at a low frequency. This difference is due to the finite dimensions of the composite in the numerical model. Indeed, by reducing the distance d between the loop and the sample, and between the sample and the measuring point, or by increasing the radius of the sample, the difference between analytical and numerical results decreases, as shown in Figure 7a,b respectively. For a low frequency (<10 kHz), this difference is around 1.9, 0.9, and 0.3 dB for a distance d of 3, 2, and 1 cm, respectively. Reducing the sample radius in the numerical model deviates from the infinite plane assumption in the

Moser model, and the difference is then greater at around 6.5, 3.1, and 0.9 dB, respectively, for a sample radius of 5, 7, and 10.5 cm.

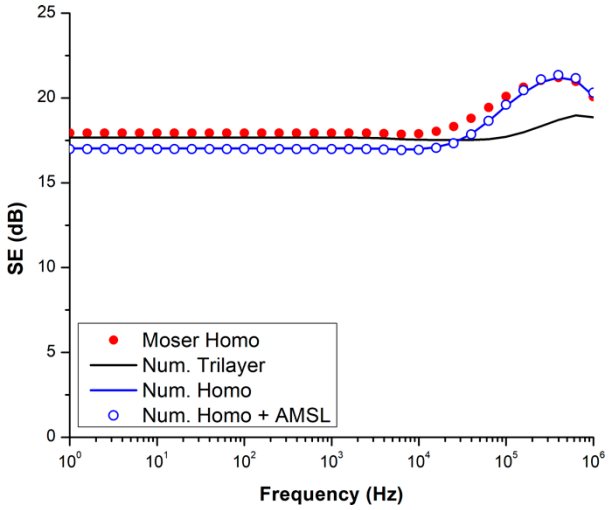

Figure 6. Shielding effectiveness of the homogenized layer (red dot) obtained with Moser model, and of the trilayer composite (black), the homogenized layer (blue), and the artificial layer (blue dot) obtained in near-field with the numerical model.

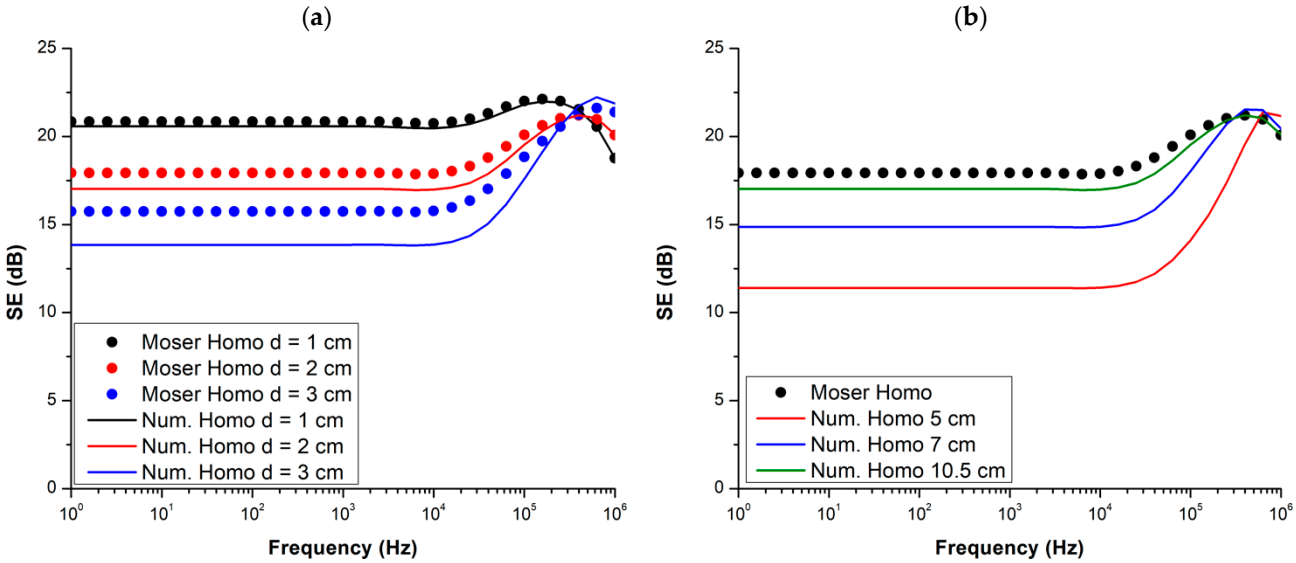

Figure 7. Shielding effectiveness of the homogenized layer obtained with Moser model (dot) and numerically (line) in near-field for different distances d with a sample radius of 10.5 cm (**a**), and for different sample radius with a distance d of 2 cm (**b**).

Comparing the numerical results, the SE of the actual trilayer composite is slightly higher, around 0.6 dB, at low frequencies than the SE of the homogenized layer. It is observed that this difference can be reduced by increasing the distance d, as shown in Figure 8. For a low frequency (<10 kHz), this difference is around 1.1, 0.6, and 0.3 dB, respectively, for a distance d of 1, 2, and 3 cm. It can also be noted that the conductivity of the graphene layer is not sufficient to compensate for the decrease in the SE for higher frequencies when the emitting loop is close to the sample (d = 1 cm). The graphene layer is more impactful for higher distances.

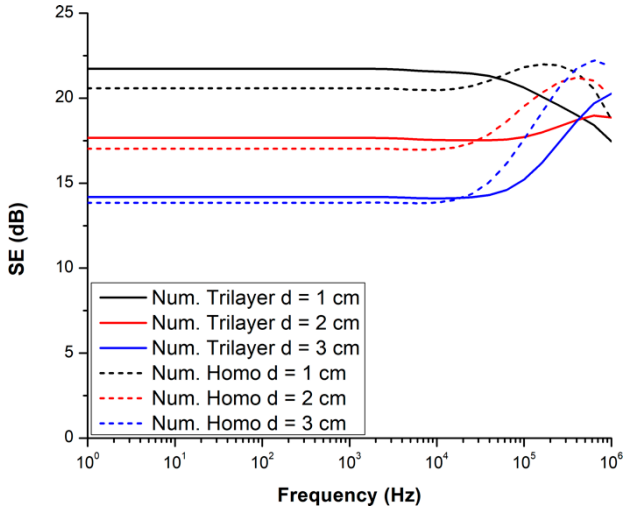

Figure 8. Shielding effectiveness of the trilayer composite (line) and the homogenized layer (dotted line) obtained numerically in near-field for different distances d with a sample radius of 10.5 cm.

Above 20 kHz, when the skin depth of the homogenized layer begins to be smaller than 2 mm, the SE of this layer rises more rapidly than the ones for the trilayer composite. This indicates that the homogenization method is less suitable for high frequencies when the skin depth is too thin compared to the total composite thickness.

The SE of the artificial layer is identical to the homogenized layer for the whole studied frequency range (see Figures 6 and 9). As in the case of homogenization only, the AMSL method is then also limited to a low frequency when the skin depth is not too thin. However, both homogenization and AMSL methods allow for reducing the calculation time. Indeed, the calculation time with the trilayer composite is around 30 min, reduced to 8 min with the homogenized layer, and to only a few seconds with the artificial layer (processor: Intel(R) Core(TM) i5-8265U CPU @ 1.60 GHz, 8GB RAM).

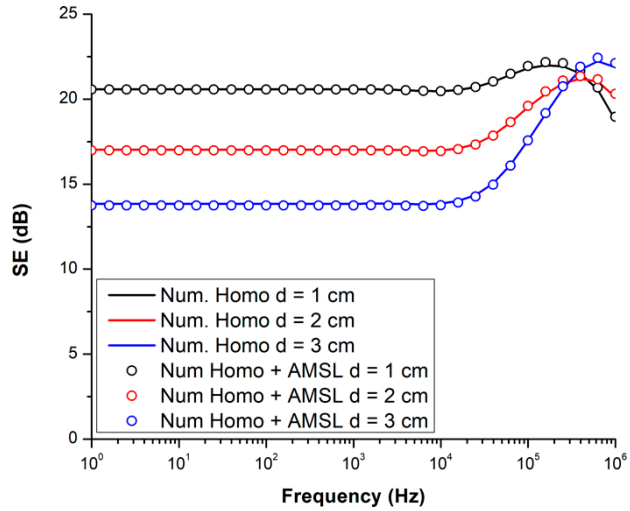

Figure 9. Shielding effectiveness of the homogenized layer (line) and the artificial layer (dot) obtained numerically in near-field for different distances d for a sample radius of 10.5 cm.

For the far-field study, the SE obtained analytically with Schelkunoff decomposition and numerically, plotted in Figure 10, are identical for both the trilayer and homogenized layer since both methods considered an infinite plane.

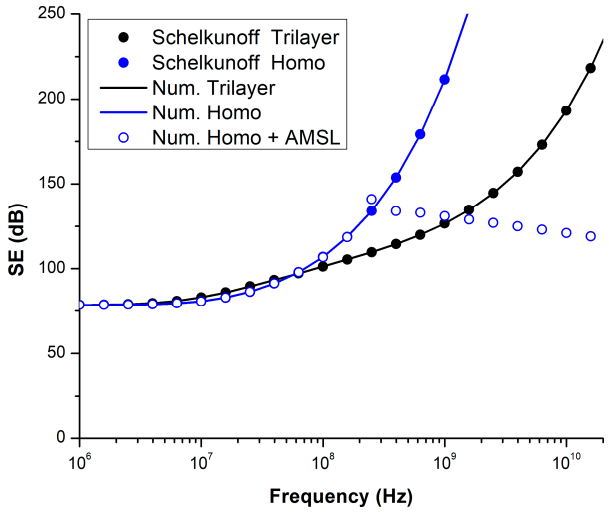

Figure 10. Shielding effectiveness of the trilayer composite (black dot) and the homogenized layer (blue dot) obtained with Schelkunoff decomposition, and the trilayer composite (black line), the homogenized layer (blue line), and the artificial layer (blue/white dot) obtained in far-field with the numerical model.

However, as observed in the near-field approach, the SE of the homogenized layer increases more rapidly with the frequency than the trilayer one, indicating that the homogenization method is not suitable for high frequencies (>60 MHz). Similarly, the AMSL method is not appropriate for high frequencies (>250 MHz).

3.5. Iso-Mass Study

The SE of the trilayer composite is now compared in an iso-mass study to the SE of aluminum (Al) and steel layers. The conductivity is set to 37.74×10^6 and 9×10^6 S/m for the Al and steel sheets, respectively. The relative permeability of steel is fixed to 200. The mass density of the trilayer composite, the Al, and steel layers are 2.55, 2.71, and 7.85 g/cm^3, respectively. Then, the thickness of Al and steel corresponding to an equal mass is 1.974 mm and 652 µm, respectively. The SE of each studied material, calculated in the near-field, is plotted in Figure 11.

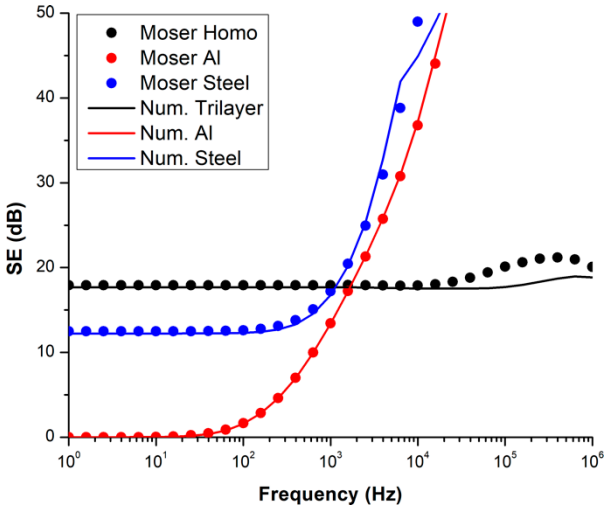

Figure 11. Shielding effectiveness at iso-mass obtained with the Moser model (dot) and numerically (line) of the trilayer composite (black), the aluminum layer (red), and the steel layer (blue).

The SE calculated with the Moser model and numerically are close for both Al and steel layers. As the steel is magnetic, a slight difference, less than 0.3 dB, is observed at a low frequency (<100 Hz). Due to their high conductivity, the SE of Al and steel layers increase quickly with the frequency. However, the trilayer composite has a higher SE until 1 kHz. Furthermore, its SE is always superior to 17 dB for the whole studied frequency range. In comparison, the SE of Al and steel layers exceeds 17 dB from around 1.5 and 1 kHz, respectively.

In the far-field, Al and steel layers are expected to show greater SE than the trilayer composite due to their higher conductivities.

4. Conclusions

In conclusion, the proposed composite demonstrates good shielding capacity on a wide frequency range, meeting the requirements due to Electromagnetic Compatibility (EMC) constraints. Indeed, the trilayer composite constituted by a graphene layer of 50 µm, a glass-fiber-reinforced epoxy of 2 mm, and a mu-ferro layer of 23 µm, has an SE higher than 17 dB and 75 dB in the near-field and far-field approaches, respectively. Separating the conductive layer and the magnetic layer with the support layer is beneficial for high frequency shielding. In the near-field approach, the graphene layer allows for compensating for the decrease in SE due to the diminution of the mu-ferro permeability for frequencies higher than 20 kHz. The results of numerical models for the simple case of plane materials are conclusive and close to analytical models. Then, the development of a numerical model with more complex geometries can be considered. The homogenization and AMSL methods are more suitable for near-field applications. These two methods can also greatly reduce the calculation time. The use of both methods may be necessary, especially for future 3D numerical models involving practical enclosures. Fabrication of the trilayer composite and experimental tests are in progress.

Author Contributions: Conceptualization and methodology, all authors; software, P.C.; validation, P.C., O.D., C.G., D.H. and L.P. (Laurent Prévond); writing—original draft preparation, P.C.; writing—review and editing, all authors. All authors have read and agreed to the published version of the manuscript.

Funding: This work benefited from the financial support of the LabEx LaSIPS (ANR-10-LABX-0032-LaSIPS) managed by the French National Research Agency under the "Investissements d'avenir" program (ANR-11-IDEX-0003).

Conflicts of Interest: The authors declare no conflict of interest.

References

1. Chen, X.; Liu, L.; Liu, J.; Pan, F. Microstructure, electromagnetic shielding effectiveness, and mechanical properties of Mg-Zn-Y-Zr alloys. *Mater. Des.* **2015**, *65*, 360–369. [CrossRef]
2. Park, J.; Lee, J.W.; Choi, H.J.; Jang, W.G.; Kim, T.S.; Suh, D.S.; Jeong, H.Y.; Chang, S.Y.; Roh, J.C.; Yoo, C.S.; et al. Electromagnetic interference shielding effectiveness of sputtered NiFe/Cu multi-layer thin film at high frequencies. *Thin Solid Films* **2019**, *677*, 130–136. [CrossRef]
3. Matsuzawa, S.; Kojima, T.; Mizuno, K.; Kagawa, K.; Wakamatsu, A. Electromagnetic simulation of low-frequency magnetic shielding of a welded steel plate. *IEEE Trans. Electromagn. Compat.* **2021**, *63*, 1896–1903. [CrossRef]
4. Arellano, Y.; Hunt, A.; Haas, O.C.L. Evaluation of near-field electromagnetic shielding effectiveness at low frequencies. *IEEE Sens. J.* **2019**, *19*, 121–128. [CrossRef]
5. Joo, K.; Lee, K.J.; Sung, H.J.; Seung, J.L.; Jeong, S.Y.; Park, H.H.; Kim, Y.H. Evaluation of package-level EMI shielding using conformally coated conductive and magnetic materials in low and high frequencies range. In Proceedings of the 2020 IEEE 70th Electronic Components and Technology Conference (ECTC), Orlando, FL, USA, 3–30 June 2020; pp. 647–652. [CrossRef]
6. Clérico, P.; Mininger, X.; Prévond, L.; Baudin, T.; Herlbert, A.-L. Compromise between magnetic shielding and mechanical strength of thin Al/steel/Al sandwiches produced by cold roll bonding: Experimental and numerical approaches. *J. Alloys Compd.* **2019**, *798*, 67–81. [CrossRef]
7. Clérico, P.; Mininger, X.; Prévond, L.; Baudin, T.; Herlbert, A.-L. Magnetic shielding of a thin Al/steel/Al composite. *COMPEL* **2020**, *39*, 595–609. [CrossRef]
8. Ma, X.; Zhang, Q.; Luo, Z.; Lin, X.; Wu, G. A novel structure of Ferro-Aluminum based sandwich composite for magnetic and electromagnetic interference shielding. *Mater. Des.* **2016**, *89*, 71–77. [CrossRef]

9. Watanabe, A.O.; Raj, P.M.; Wong, D.; Mullapudi, R.; Tummala, R. Multilayered electromagnetic interference shielding structures for suppressing magnetic field coupling. *J. Electron. Mater.* **2018**, *47*, 5243–5250. [CrossRef]
10. Nisanci, M.H.; de Paulis, F.; Di Febo, D.; Orlandi, A. Sensitivity analysis of electromagnetic transmission, reflection and absorption coefficients for biphasic composite structures. In Proceedings of the 2014 International Symposium on Electromagnetic Compatibility, Gothenburg, Sweden, 1–4 September 2014; pp. 438–443. [CrossRef]
11. Liu, P.S.; Qing, H.B.; Hou, H.L.; Wang, Y.Q.; Zhang, Y.L. EMI shielding and thermal conductivity of a high porosity reticular titanium foam. *Mater. Des.* **2016**, *92*, 823–828. [CrossRef]
12. Kim, S.S.; Kim, S.T.; Yoon, Y.C.; Lee, K.S. Magnetic, dielectric, and microwave absorbing properties of iron particles dispersed in rubber matrix in gigahertz frequencies. *J. Appl. Phys.* **2005**, *97*, 10F905. [CrossRef]
13. Jalali, M.; Dauterstedt, S.; Michaud, A.; Wuthrich, R. Electromagnetic shielding of polymer-matrix composites with metallic nanoparticles. *Compos. Part B* **2011**, *42*, 1420–1426. [CrossRef]
14. Jianzhong, W.; Jun, M.; Hao, Z.; Huiping, T. Preparation and electromagnetic shielding effectiveness of metal fibers/polymer composite. *Rare Met. Mater. Eng.* **2017**, *46*, 73–77. [CrossRef]
15. Darques, M.; Spiegel, J.; De La Torre Medina, J.; Huynen, I.; Piraux, L. Ferromagnetic nanowire-loaded membranes for microwave electronics. *J. Magn. Magn. Mater.* **2009**, *321*, 2055–2065. [CrossRef]
16. Qin, F.X.; Peng, H.X.; Pankratov, N.; Phan, M.H.; Panina, L.V. Exceptional electromagnetic interference shielding properties of ferromagnetic microwires enabled polymer composites. *J. Appl. Phys.* **2010**, *108*, 044510. [CrossRef]
17. Xu, Y.L.; Uddin, A.; Estevez, D.; Luo, Y.; Peng, H.X.; Qin, F.X. Lightweight microwire/graphene/silicone rubber composites for efficient electromagnetic interference shielding and low microwave reflectivity. *Compos. Sci. Technol.* **2020**, *189*, 108022. [CrossRef]
18. Liu, Y.; He, D.; Dubrunfaut, O.; Zhang, A.; Zhang, H.; Pichon, L.; Bai, J. Go-CNTs hybrids reinforced epoxy composites with porous structure as microwave absorbers. *Compos. Sci. Technol.* **2020**, *200*, 108450. [CrossRef]
19. Fan, X.; Zhang, G.; Li, J.; Shang, Z.; Zhang, H.; Gao, Q.; Qin, J.; Shi, X. Study on foamability and electromagnetic interference shielding effectiveness of supercritical CO_2 foaming epoxy/rubber/MWCNTs composite. *Compos. Part A* **2019**, *121*, 64–73. [CrossRef]
20. Xie, Y.; Li, Z.; Tang, J.; Li, P.; Chen, W.; Liu, P.; Li, L.; Zheng, Z. Microwave-assisted foaming and sintering to prepare lightweight high-strength polystyrene/carbon nanotube composite foams with an ultralow percolation threshold. *J. Mater. Chem. C* **2021**, *9*, 9702–9711. [CrossRef]
21. Chung, D.D.L.; Eddib, A.A. Effect of fiber lay-up configuration on the electromagnetic interference shielding effectiveness of continuous carbon fiber polymer-matrix composite. *Carbon* **2019**, *141*, 685–691. [CrossRef]
22. Ameli, A.; Jung, P.U.; Park, C.B. Electrical properties and electromagnetic interference shielding effectiveness of polypropylene/carbon fiber composite foams. *Carbon* **2013**, *60*, 379–391. [CrossRef]
23. Song, W.L.; Cao, M.S.; Lu, M.M.; Bi, S.; Wang, C.Y.; Liu, J.; Yuan, J.; Fan, L.Z. Flexible graphene/polymer composite films in sandwich structures for effective electromagnetic interference shielding. *Carbon* **2014**, *66*, 67–76. [CrossRef]
24. Moser, J.R. Low frequency shielding of a circular loop electromagnetic field source. *IEEE Trans. Electromagn. Compat.* **1967**, *9*, 6–18. [CrossRef]
25. Schelkunoff, S.A. *Electromagnetic Waves*; Bell Telephone Laboratories Series; Van Nostrand: New York, NY, USA, 1943.
26. Kühn, M.; John, W.; Weigel, R. Analytical calculation of intrinsic shielding effectiveness for isotropic and anisotropic materials based on measured electrical parameters. *Adv. Radio Sci.* **2014**, *12*, 83–89. [CrossRef]
27. Cruciani, S.; Campi, T.; Maradei, F.; Feliziani, M. Conductive layer modeling by improved second-order artificial material single-layer method. *IEEE Trans. Antennas Propag.* **2018**, *66*, 5646–5650. [CrossRef]
28. Holland Shielding Systems BV. 2021. Available online: https://hollandshielding.com/Mu-ferro-tape-foil (accessed on 1 June 2021).